Am J Transl Res 2022;14(9):6082-6094
www.ajtr.org /ISSN:1943-8141/AJTR0142926

Original Article

A novel ferroptosis-related gene signature to predict overall survival in patients with osteosarcoma

Junqing Li[1*], Feiran Wu[1*], Xing Xiao[2*], Li Su[1], Xinjun Guo[1], Jie Yao[1], Huimin Zhu[1]

[1]Minimally Invasive Spinal Surgery Center, Luoyang Orthopedic-Traumatological Hospital of Henan Province (Henan Provincial Orthopedic Hospital), Zhengzhou 450016, China; [2]Scientific Research Center, Seventh Affiliated Hospital, Sun Yat-sen University, Shenzhen 518000, China. [*]Equal contributors.

Received March 16, 2022; Accepted July 25, 2022; Epub September 15, 2022; Published September 30, 2022

Abstract: Objectives: Ferroptosis plays vital roles in the pathogenesis of various malignant tumors. However, knowledge on roles of ferroptosis in osteosarcoma remains scarce. In the present study, a comprehensive bioinformatics analysis was performed aiming to identify ferroptosis-related genes (FRGs), construct a FRGs-based model predicting overall survival (OS), and assess the impact of these FRGs on the migration and invasion of osteosarcoma cells. Methods: Initially, data regarding differentially expressed FRGs were obtained from the GSE160881 dataset. Prognostic significance and possible biological functions of these differentially expressed FRGs were comprehensively and systematically explored adopting a series of bioinformatics methods. The impact of cystathionine β-synthase (CBS) on migration and invasion of osteosarcoma cells were assessed using transwell assays. Results: A total of 50 FRGs were differentially expressed. Four FRGs including *G6PD*, *VEGFA*, *CBS*, and *HMOX1* were used to construct a model predicting OS in osteosarcoma patients. In the training cohort, patients with high risk had significantly poorer OS than those with low risk, which was also demonstrated in validation cohorts (GSE16091 and GSE39058). Furthermore, we established a clinically useful nomogram predicting OS using the four FRGs mentioned above. Risk scores were significantly associated with the proportion of tumor-infiltrating immune cells. Additionally, we used the Cytoscape software to identify hub FRGs, and found that *TP53*, *HMOX1*, *SLC7A11*, *HRAS*, *VEGFA*, and *TXNRD1* were hub FRGs. By performing *in vitro* cell culture experiments, we demonstrated that invasion and migration capability of Saos2 and HOS cells were significantly weakened after CBS knock down. Conclusions: In conclusion, gene signatures based on four FRGs were reliable in predicting OS in patients with osteosarcoma. Findings from this study will enable a better understanding of the prognostic significance of FRGs and tumor immunity in osteosarcoma.

Keywords: Osteosarcoma, ferroptosis-related genes, tumor immunity, cystathionine β-synthase

Introduction

Among children and adolescents, osteosarcoma is the most common malignant tumor of the bone [1, 2]. The rather poor prognoses in patients with osteosarcoma is mainly due to the predisposition of osteosarcoma to metastasize, especially to the lung [3]. Despite the advances made in chemotherapy, neoadjuvant chemotherapy, and immunotherapy for patients with osteosarcoma, long-term prognoses in these patients remain rather poor [1, 2, 4]. Therefore, seeking novel biomarkers and elucidating the possible mechanisms involved remains urgent since it would enable researchers to develop brand new therapeutic strategies and improve prognosis.

Ferroptosis is characterized by an iron-dependent abnormal accumulation of lipid hydroperoxides at lethal levels [5]. According to some previously published studies, ferroptosis kills cancer cells and also plays vital roles in the pathogenesis of malignant tumors [6-8]. Furthermore, in these studies, inducing ferroptosis has been suggested as a potential therapeutic strategy triggering death in cancer cells [6-8]. With the growing number of published studies investigating ferroptosis, the number of known genes modulating ferroptosis and biomarkers for ferroptosis is increasing remarkably. For example, it was reported that through suppressing the expression of *SLC7A11*, p53 could increase the sensitivity of cancer cells to ferroptosis [9]. In human hepatocellular carci-

noma cells, activation of the p62-Keap1-NRF2 pathway prevents ferroptosis [10]. In human pancreatic ductal adenocarcinoma cells, ferroptosis was prevented by *HSPA5* expression through increased stability of *GPX4* [11]. Inhibition of *HSF1* and *HSFB1* could suppress growth of tumor cells through increasing the accumulation of iron and reactive oxygen species (ROS) within tumor cells [12]. Additionally, a series of FRGs significantly associated with prognoses in patients with various tumors such as lung cancer [13], melanoma [14], ovarian cancer [15], and glioma [16] have been identified. Therefore, ferroptosis may also play crucial roles in pathogenesis and progression of osteosarcoma and a comprehensive study investigating roles played by ferroptosis will potentially help us develop novel therapeutic strategies and improve survival in patients with osteosarcoma.

In the present study, mRNA expression profiles of FRGs and corresponding clinical information of osteosarcoma patients were obtained from public databases. Then a prognostic signature utilizing multiple FRGs in TCGA was established and this model was validated in the GEO cohort. Subsequently, the correlations between FRGs and tumor immunity were evaluated. Ultimately, findings of this study were further validated by *in vitro* experiments.

Materials and methods

Data processing

The relevant data for 366 FRGs (Table S1) were extracted from the FerrDb database (http://www.datjar.com:40013/bt2104/), including drivers, suppressors, and markers. Differentially expressed genes (DEGs) between normal and osteosarcoma tissues derived from RNA-seq data of GSE16088 [17] were identified using the "limma" package [18]. Genes whose *p*-values were <0.05 and log2|fold change| values >1 were defined as DEGs. The "ggplot2" packages [19] and the "pheatmap" packages [20] were used to create volcano plots and heatmaps respectively.

Data of the training cohorts were obtained from TARGET (https://ocg.cancer.gov/) and TCGA databases. Data of the validation cohorts (GSE16091 [17] and GSE39058 [21]) including RNA-seq and corresponding clinical datasets were obtained from GEO database.

Construction and validation of a FRGs signature

Initially, data regarding clinical information and mRNA expression were extracted from TCGA and TARGET. Univariate Cox regression analysis was performed to identify FRGs with prognostic significance. The risk of overfitting was minimized through constructing a prognostic model by performing LASSO Cox regression analysis. Variable selection and shrinkage were accomplished adopting the LASSO algorithm using the "glmnet" R package. Risk score (RS) was computed and evaluated using the following equation: $RS = coef_{gene1} \times Exp_{gene1} + coef_{gene2} \times Exp_{gene2} + coef_{genei} \times Exp_{genei}$. Based on the median RS, patients were correspondingly assigned into the high-risk group or low-risk group. Log-rank test was performed to compare OS between two groups. Predictive capability of the model mentioned above was evaluated by plotting the receiver operating characteristic (ROC) curve using survival ROC package. Additionally, RS of patients from the validation cohort were calculated adopting the prognostic model obtained from the training cohort. In a similar way, ROC curves and survival curves of the validation cohort were plotted and visualized using the methods mentioned above. Ultimately, a nomogram was constructed to predict OS using the "rms" package more intuitionally and conventionally.

Tumor-infiltrating immune cell analysis and immune scores

The CIBERSORT tool [22] was used to assess tumor-infiltrating immune cells (TIICs) in TARGET datasets. The abundance ratio matrix of the 22 immune cells was obtained at $P<0.05$. The immune and stromal scores of the samples from the TARGET datasets were calculated adopting the ESTIMATE algorithm.

GO enrichment, KEGG pathway, and gene set variation analyses

Then by adopting the R software "clusterProfiler" package [23], we conducted KEGG pathway analyses and GO enrichment analyses, results of which were plotted using the "ggplot2" packages. The GSVA package of R was adopted to

estimate variations of key gene sets [24]. A gene expression matrix was used as the input for the GSVA algorithm to non-parametrically calculate GSVA scores.

Identification of Hub genes and biological networks

Data in terms of protein-protein interaction (PPI) networks of differentially expressed FRGs were obtained from the STRING database. The PPI network was plotted and visualized using Cytoscape 3.7.2 software. As two topological features of the PPI network, degree and betweenness were used to determine potential hub genes. Of the identified hub genes, the first 10 were selected and corresponding PPI networks of these ten hub genes were constructed. NetworkAnalyst 3.0 was utilized to establish a transcription factor-microRNA (miRNA) co-regulatory network of prognosis-related genes and hub genes.

Cell culture and transfection

We purchased Saos2 and HOS cell lines from the Cell Bank of the Chinese Academy of Sciences (Shanghai, China). Both cell lines were cultured in DMEM (Biological Industries, Shanghai, China) containing 10% FBS (Biological Industries, Shanghai, China). RiboBio (Guangzhou, China) was responsible for designing and synthesizing the siRNA and negative control siRNA oligonucleotides adopted in this study. Detailed information regarding sequences of si-1 and si-2 is presented in Table S2. According to the instructions provided by the manufacturer, we then performed siRNA transfections using the Ribo FECT™CP Transduction Kit (RiboBio).

Quantitative real-time PCR and western blotting

Quantitative Real-Time PCR (RT-PCR) and Western Blotting (WB) was conducted as the manufacturer's instructions and previously described [25]. RT-PCR reagents including AG RNAex Pro Reagent, SYBR Green Premix Pro Taq HS qPCR Kit and Evo M-MLV RT Premix Kit were purchased from Accurate Biology (Changsha, China). Detailed information of primer sequences is listed in Table S2. WB reagents including RIPA buffer and BeyoECL Plus Kit were purchased from Beyotime Biotechnology (Shanghai, China). Anti-GAPDH (10494-1-AP) and anti-CBS (14787-1-AP) antibodies were purchased from Proteintech corporation (Wuhan, China).

Cell migration and invasion assays

We performed transwell assays with the aim of further assessing the impact of CBS expression on migration and invasion of Saos2 and HOS cells. For transwell assays assessing migration, 5×10^4 cells were plated into the upper chamber containing serum-free medium (8 μm pore size, Corning, NY, USA) while 10% FBS-supplemented medium was added into the lower chamber. Transwell assays assessing invasion were the same as transwell assays assessing migration except that the upper chamber was pre-coated with 10% Matrigel (Corning). After 36 hours of incubation, cells remaining in the upper chamber were rubbed off using swabs. Cells that passed through the membrane were chemically fixed using 4% paraformaldehyde and then stained using 0.1% crystal violet. Cells having migrated into the lower chamber were counted in five different fields using a microscope.

Statistical analysis

In this study, most bioinformatics and statistical analyses were accomplished by R software including normalization and transformation of RNA-seq data, DEG analysis, ROC analysis, survival analysis, CIBERSORT, ESTIMATE, and GSVA. All quantitative data from *in vitro* experiments were demonstrated as mean ± standard deviation of three independent experiments. One-way ANOVA analysis was performed using GraphPad Prism 8.0 (GraphPad, La Jolla, CA, USA) to analyze differences among three groups. Analyses whose *P* values were <0.05 were considered as statistically significant.

Results

Differentially expressed FRGs in osteosarcoma

The "limma" package was adopted to identify differentially expressed FRGs in GSE16088 that included normal bone and osteosarcoma tissues. A heatmap illustrating FRG expression in GSE16088 was then established, which is presented in **Figure 1A**. Ultimately, a total of 50 FRGs were identified as DEGs from 366 FRGs,

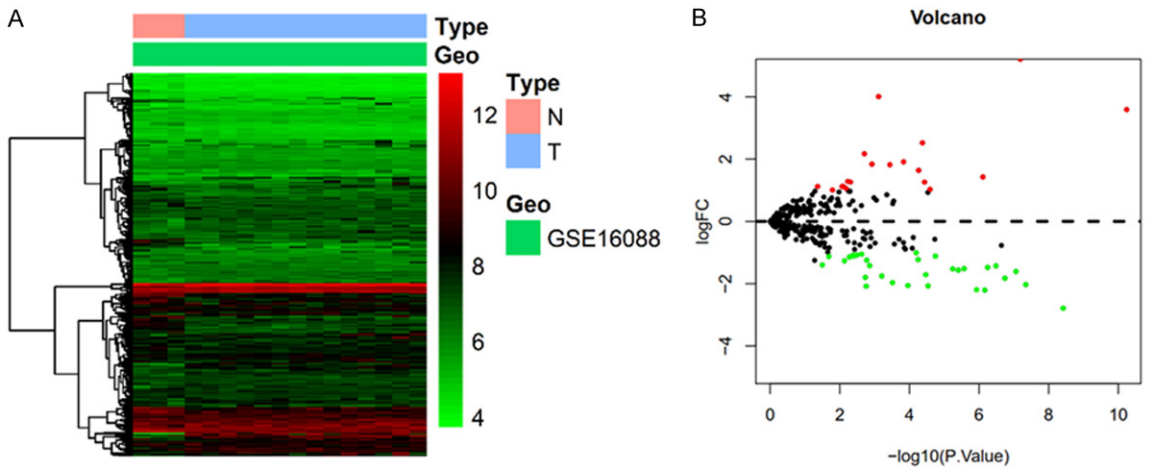

Figure 1. Heatmap and volcano plot of 366 ferroptosis-related genes in normal bone tissues and osteosarcoma tissues from GSE16088. A. Heatmap. B. Volcano plot.

of which 31 were down-regulated and 19 were up-regulated (**Figure 1B**; Table S3).

Construction of a novel prognostic FRG signature based on LASSO

With the purpose of assessing the effects of FRGs expression on long-term outcomes in patients with osteosarcoma, we initially conducted univariate Cox analysis to identify variables significantly associated with OS, results of which revealed that five candidate FRGs were significantly associated with OS (**Figure 2A**). To further verify key genes significantly associated with prognosis of osteosarcoma patients, we used the "glmnet" package to accomplish LASSO regression analysis. Then we established the model adopting the method of five-fold cross-validation. The corresponding confidence interval for each lambda is demonstrated in **Figure 2B** and the trajectory of the coefficient for each gene with a value of in (lambda) is presented in **Figure 2C**. Four genes were chosen as signature genes for the model.

RS was calculated using the following formula: (-0.645 × Exp G6PD) + (0.232 × Exp VEGFA) + (0.597 × Exp CBS) + (-0.105 × Exp HMOX1). Then we assigned patients from the training cohort (TARGET) into the high-risk group or the low-risk groups according to the median RS. It was revealed by survival analysis that in comparison with patients with low risk, those with high risk had worse OS (**Figure 2D**). The expression heatmap of these FRGs and the survival status and RS of the patients in the OS model are presented in **Figure 2E**. To further assess the predictive capabilities of the FRGs mentioned above, we then accomplished time-dependent receiver operating curve analyses, results of which revealed that the area under the ROC curve (AUC) for this OS predictive model was 0.782, 0.811, and 0.877 at 3, 5, and 7 years, respectively (**Figure 2F**).

Robustness of the Four-Gene Signature Model Verified by External Datasets

To further validate the predictive capability of the model mentioned above, we then performed verification analysis using the GSE16091 and GSE39058 datasets. As with the results of the training cohort, it was revealed that in comparison with patients with low risk, those with high risk had worse OS (**Figure 3A**). The expression heatmap of these FRGs and the survival status and RS of the patients in the OS model are presented in **Figure 3B**. The AUCs for this OS predictive model were 0.741, 0.737, and 0.703 at 3, 5, and 7 years, respectively (**Figure 3C**). In conclusion, four FRGs were determined, and a model based on these four genes that could reliably predict OS in patients with osteosarcoma was established.

Building a predictive nomogram

The prognostic value of the RS model and other clinical parameters was subsequently evaluated by accomplishing both univariate and multivariate Cox analyses, results of which demonstrated that for patients in the TARGET dataset

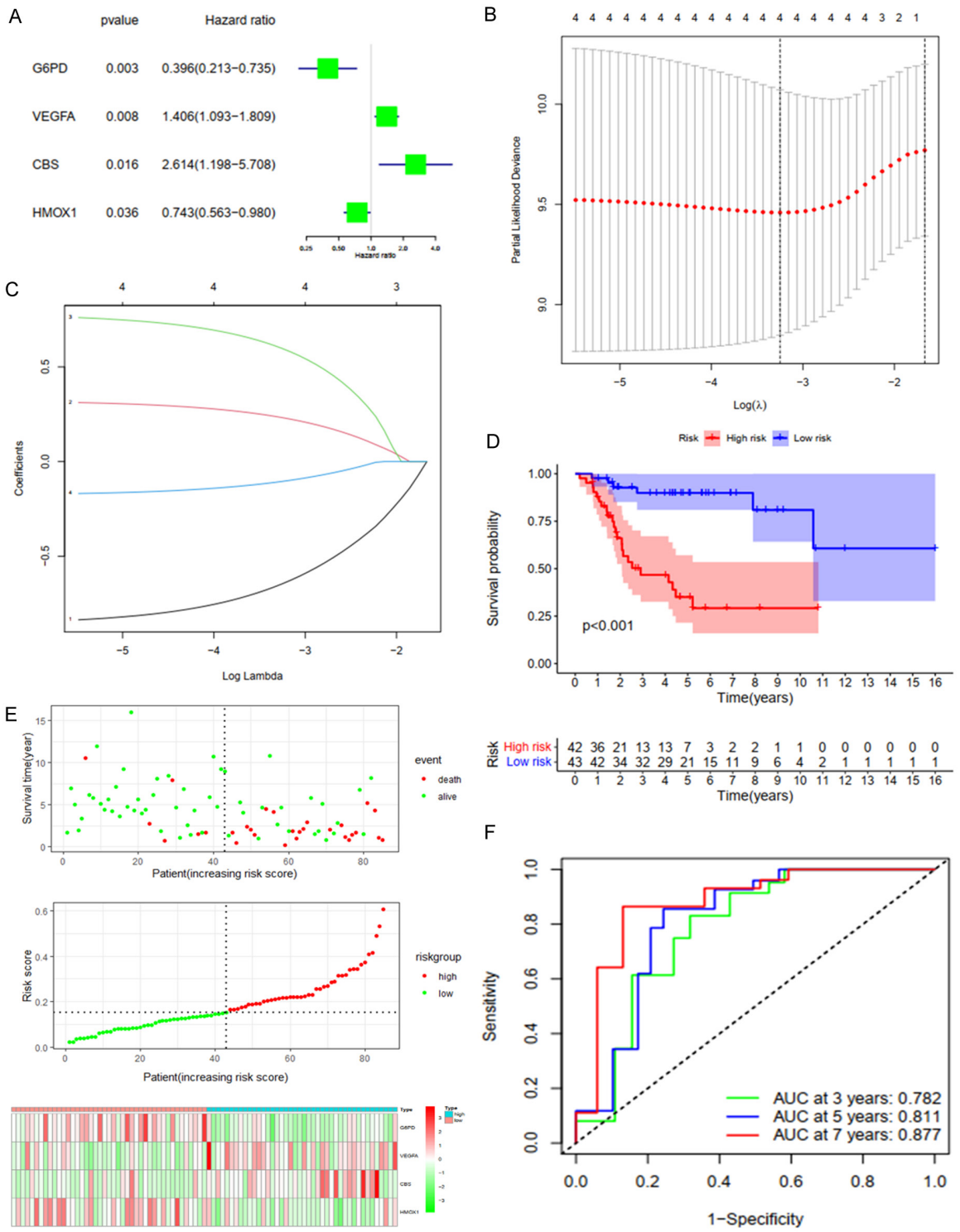

Figure 2. Development of the overall survival (OS)-prediction model for osteosarcoma. A. Univariate COX regression analysis of OS in training cohort (TARGET). B. Partial likelihood deviance is plotted against log (lambda). C. Least absolute shrinkage and selection operator (LASSO) coefficient profiles of FRGs. D-F. Survival curve, survival status, risk score, heatmap, and receiver operating characteristic curve for low- and high-risk subgroups in the training cohort (TARGET).

(**Figure 4A** and **4B**), RS was an independent prognostic factor for OS. Then a nomogram of clinical utility was generated to enable us to better predict survival in patients with osteo-

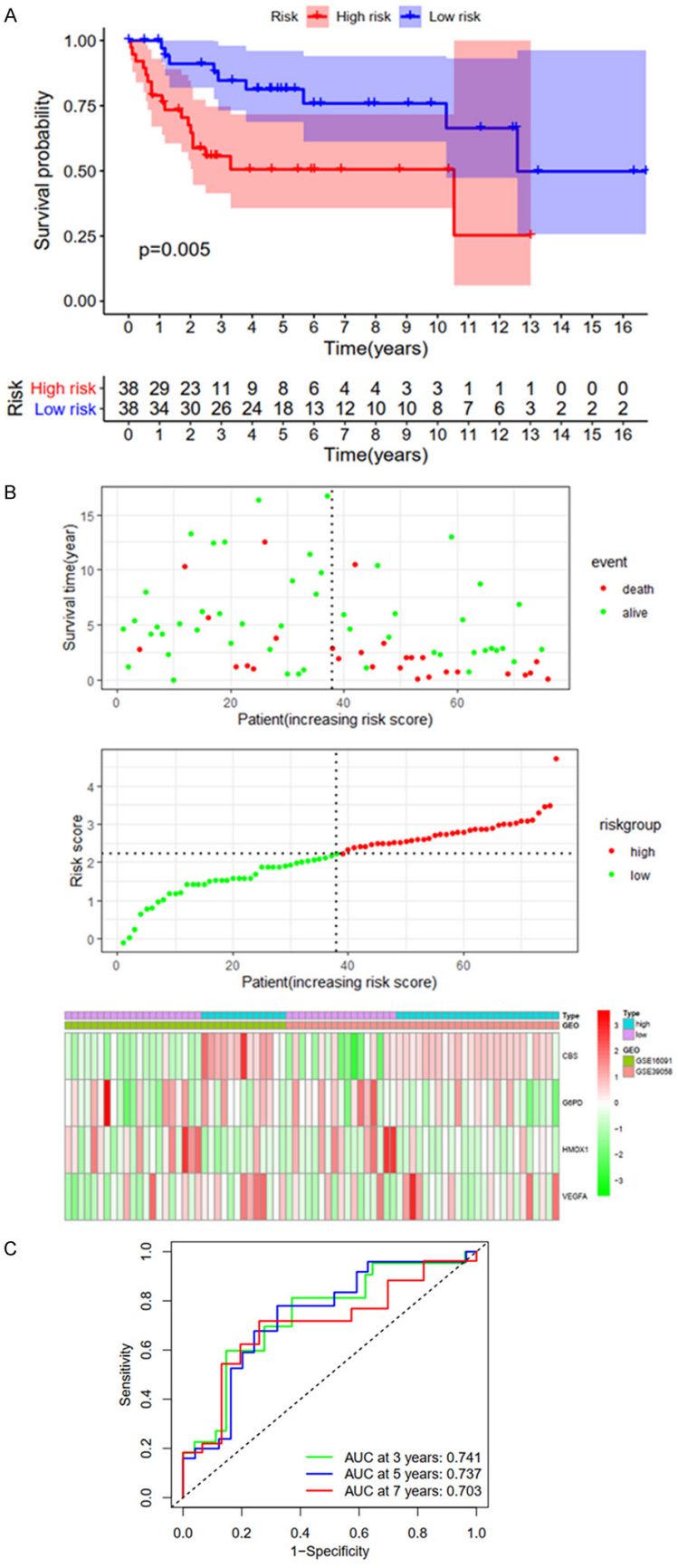

Figure 3. Validation of the overall survival-prediction model for osteosarcoma. A-C. Survival curve, survival status, risk score, heatmap, and receiver operating characteristic curve for low- and high-risk subgroups in the training cohort (GSE16091 and GSE39058).

sarcoma utilizing the four-gene signature mentioned above. We then assigned a corresponding point to each gene based on the point scale. The specific location of each gene was determined by drawing a horizontal line. Then total scores of the patients were obtained by adding all the points based on the estimated 3-, 5-, and 7-year survival rates of the patients.

Differences in immune infiltration between risk groups

Given the fact that immune infiltration significantly affected survival in patients with malignant tumors, we further used the CIBERSORT and ESTIMATE tools to assess the differences between risk groups in terms of overall immune infiltration and immune cells. Results of the CIBERSORT analysis demonstrated that in comparison with those in the high-risk group, the numbers of infiltrating CD8+ T cells and M1 and M2 macrophages in the low-risk group were significantly higher while the number of infiltrating M0 macrophages was significantly lower in the low-risk group (**Figure 5A**). The ESTIMATE results showed that the stromal and immune scores in the low-risk group were higher than those in the high-risk group (**Figure 5B**).

Subsequently, the differences between risk groups regarding

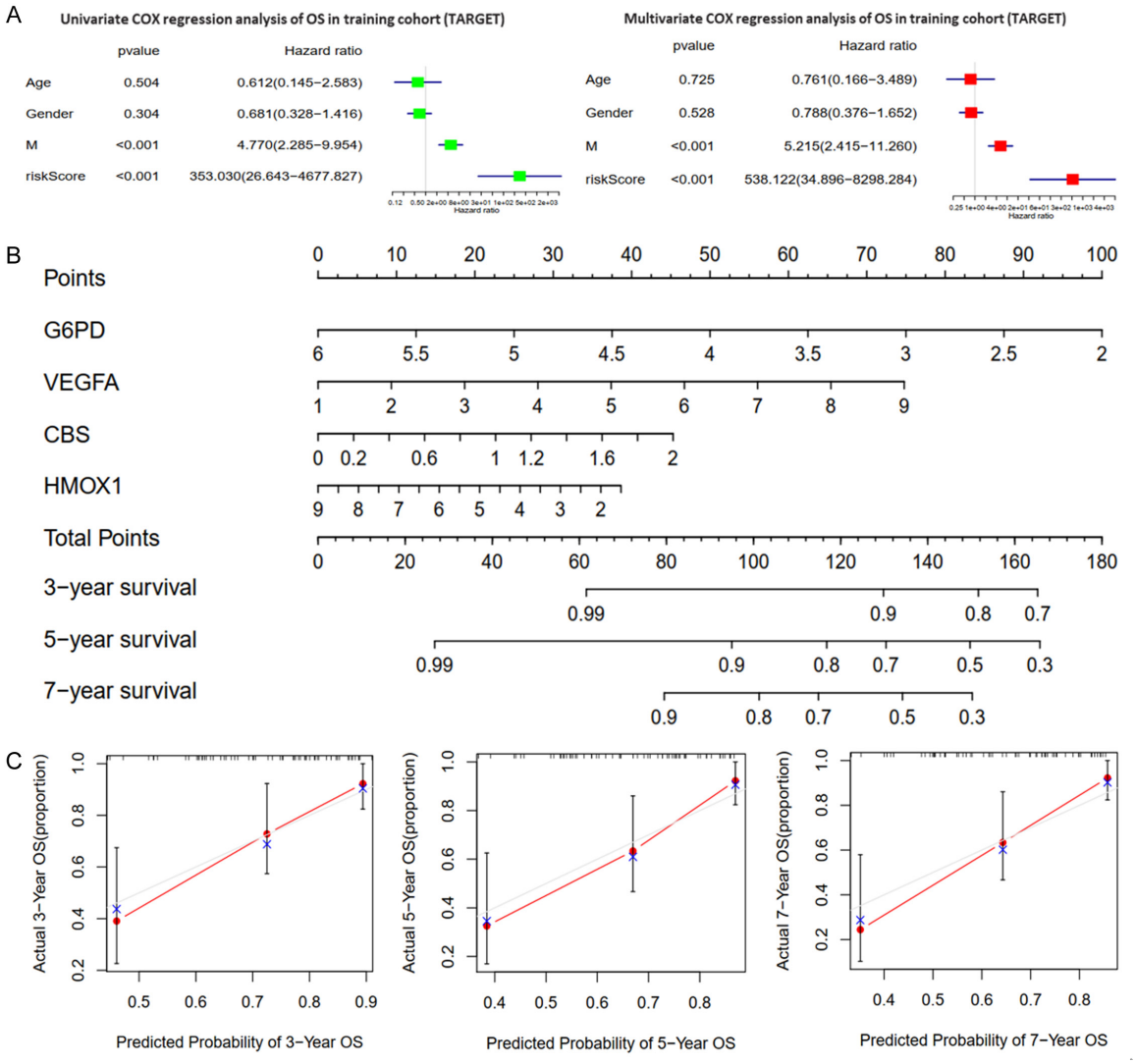

Figure 4. A nomogram for predicting 3-, 5-, and 7-year overall survival (OS) of the training cohort (TARGET). A. Univariate and multivariate COX regression analysis of OS in the training cohort (TARGET). B. Nomogram for predicting 3-, 5-, and 7-year OS. C. Calibration plots.

expression levels of some checkpoint genes were evaluated. For the high-risk group, almost all the known checkpoint genes were down-regulated. The expression levels of *CD274*, *HAVCR2*, *CTLA4*, *PDCD1*, *TIGIT*, *CD80*, *LAG3*, *CD96*, *CD86*, and *PDCD1LG2* were significantly different between risk groups (**Figure 5D**). Ultimately, the associations between TIICs, the four prognostic FRGs and the expression levels of immune checkpoint genes were explored. The expression level of *G6PD* was negatively associated with infiltration of resting mast cells while the expression level of *CBS* was positively associated with infiltration of CD8+ T cells and that of HMOX1 positively with activation of dendritic cells (**Figure 5E**). The associations between the expression levels of the four FRGs and the immune checkpoint genes are demonstrated in **Figure 5F**.

Biological functions and networks

We subsequently performed GO and KEGG analyses of these FRGs using the "clusterProfiler" package to further evaluate the functions of these aforementioned differentially expressed FRGs and the possible mechanisms through which these differentially expressed FRGs regulated the biological behavior of osteosarcoma.

As demonstrated in **Figure 6A**, these FRGs were mainly enriched and involved in the mito-

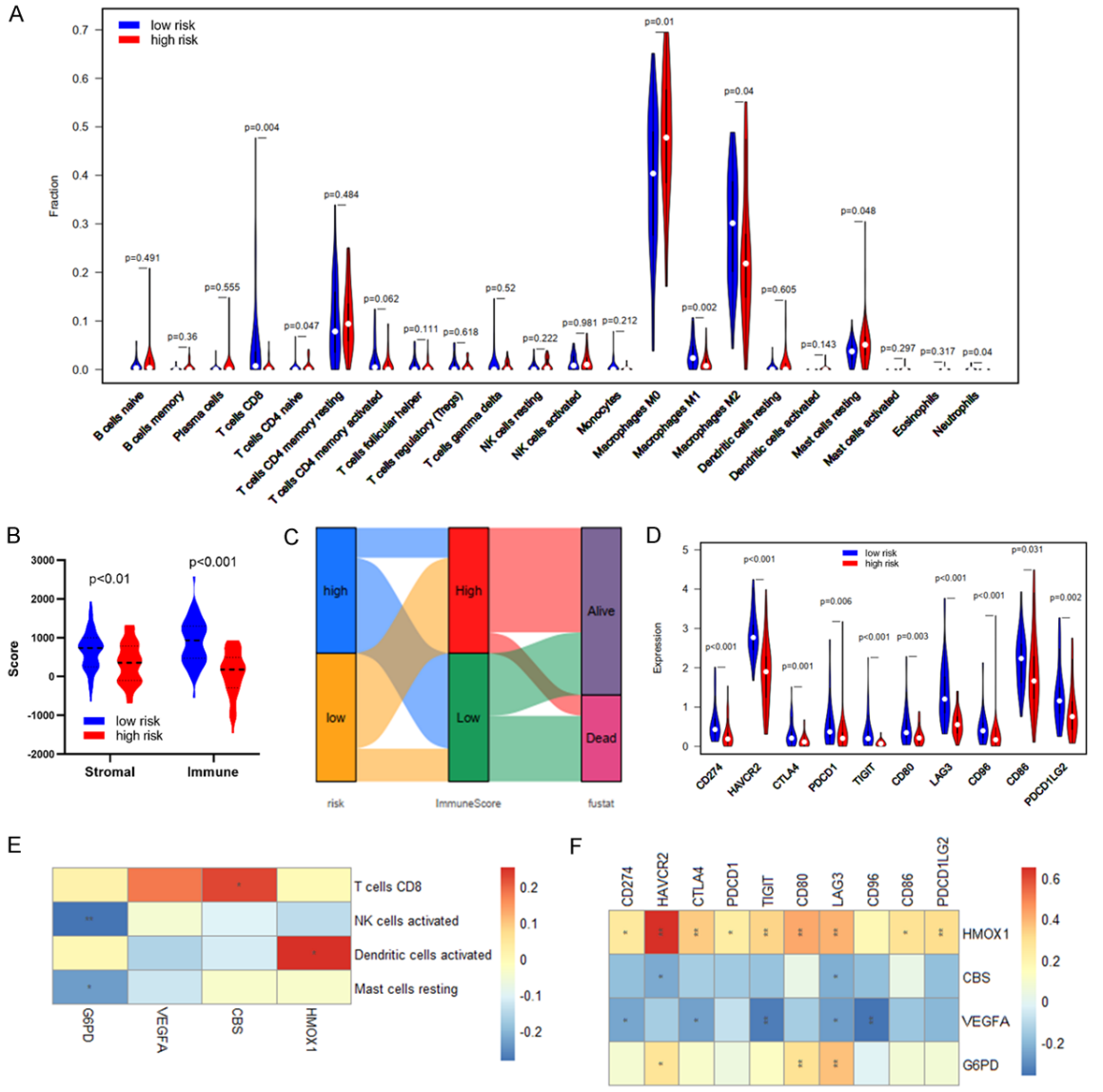

Figure 5. Immune infiltration between risk groups. A. Violin plot comparing the proportions of tumor-infiltrating immune cells (TIICs) in low- and high- risk groups in TARGET. B. Comparisons between the high- and low-risk groups in terms of stromal score and immune score. C. The Sankey diagram of risk score, immune score, and survival status. D. Differences in expression of immune checkpoint genes between low- and high-risk groups. E. Correlation heatmap of prognostic ferroptosis-related genes (FRGs) and TIICs. F. Correlation heatmap of prognostic FRGs and immune checkpoint genes. (*P<0.05, **P<0.01).

chondrial matrix, melanosome, pigment granule, oxidoreductase complex, tricarboxylic acid cycle enzyme complex, and flavin adenine dinucleotide binding. Results of biological process analysis revealed that these FRGs were involved in response to oxidative stress and hypoxia, and homeostasis in number of cells. Additionally, it was demonstrated through KEGG pathway enrichment analysis that the FRGs mentioned above participated in ferroptosis, hepatocellular carcinoma, carbon metabolism in cancer and bladder cancer (**Figure 6B**).

Then GSVA was accomplished to compare between risk groups in terms of pathways, results of which revealed that significant differences between the two groups mainly lied in antigen processing and presentation, primary immunodeficiency, NK cell-mediated cytotoxicity, lysosomes, and B cell receptor signaling pathway (**Figure 6C**).

To further investigate the potential functions of the aforementioned differentially expressed FRGs in osteosarcoma, we then used the

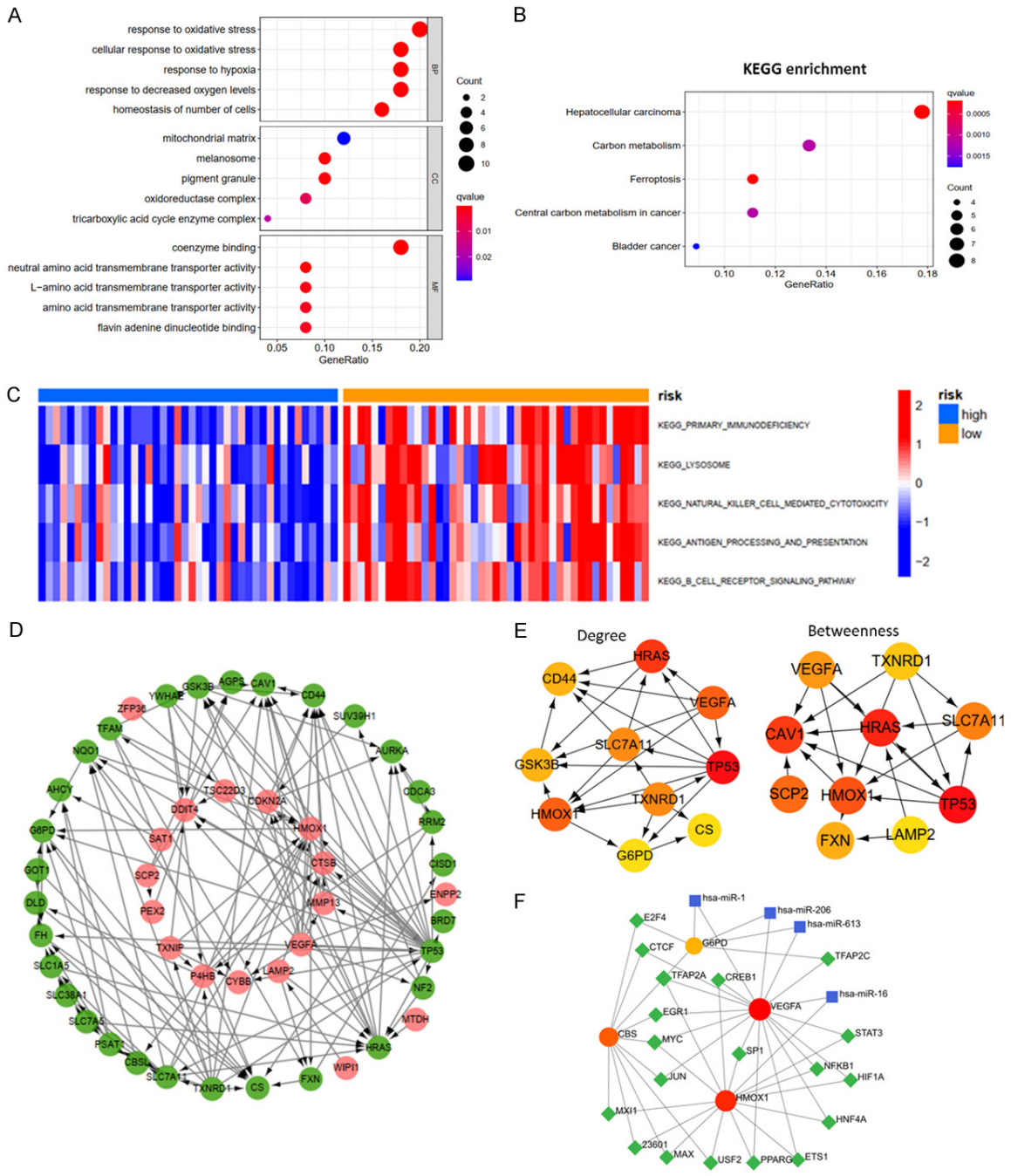

Figure 6. Biological functions and network. A, B. GO enrichment and KEGG pathway analysis of differentially expressed ferroptosis-related genes (FRGs). C. Gene set variation analysis of low- and high-risk groups in the TARGET cohort. D. Protein-protein interaction (PPI) network of differentially expressed FRGs. E. Identifying the first 10 FRGs and constructing the corresponding PPI network using the degree and betweenness topological methods. F. Transcription factor-miRNA co-regulatory network of four prognosis-related FRGs.

Cytoscape3.7.2 software (**Figure 6D**) to plot PPI networks of these FRGs. The first 10 genes were chosen to construct their corresponding PPI networks adopting the betweenness and degree topological methods (**Figure 6E**). By combining results of these two methods, we identified six hub genes that included *TP53, HMOX1, SLC7A11, HRAS, VEGFA*, and *TXNRD1*. In addition, the transcription factor-miRNA co-regulatory network of the four prognosis-related FRGs (**Figure 6F**) was constructed using NetworkAnalyst.

Invasion and migration capability of osteosarcoma cells was significantly inhibited after cbs was being knocked down

Despite the fact that CBS had been identified as a prognosis-related FRG, its roles in osteosarcoma remain ambiguous. Therefore, we conducted *in vitro* cellular experiments to evaluate the effects of CBS on osteosarcoma cells. RT-PCR (**Figure 7A**) was conducted to assess the mRNA expression of CBS in different osteosarcoma cell lines. Saos2 and HOS cells were transfected with siRNAs (si-nc, si-1, and si-2). Verified using RT-PCR and WB, it was revealed that in comparison with Saos2 and HOS cells transfected with si-nc, those transfected with si-1 or si-2 had significantly reduced levels of CBS expression (**Figure 7B**). Transwell assays revealed that both migration and invasion of Saos2 ($P<0.05$, **Figure 7C**) and HOS ($P<0.05$, **Figure 7D**) cells were significantly inhibited after CBS knock-down. Considering all these results mentioned above, we could conclude that CBS played significant roles in promoting osteosarcoma progression and might serve as a biomarker that could potentially predict prognosis in patients with osteosarcoma.

Discussion

As an iron-dependent and ROS-reliant cell death process, ferroptosis is characterized by the following cytological changes: a condensed mitochondrial membrane, decreased mitochondrial cristae, and rupture of the mitochondrial membrane [26]. The number of studies investigating the roles of ferroptosis in malignant tumors is continuously increasing and these studies have enabled to better understand the potential of ferroptosis in treating cancers. However, the roles played by ferroptosis and FRGs in osteosarcoma have not been fully explored. Therefore, a systematic study investigating the potential functions FRGs in osteosarcoma is necessary since this it will enable us to better understand novel mechanisms contributing to progression of osteosarcoma and potentially improve prognosis in patients with osteosarcoma.

Initially, we identified 50 differentially expressed FRGs from 366 FRGs. Second, prognostic significance of these differentially expressed FRGs was investigated. Third, Cox regression analysis was performed and a model that could reliably predict OS in patients with osteosarcoma was constructed. *CBS, G6PD, HMOX1*, and *VEGFA* genes were selected to establish this predictive model. By performing ROC analysis, we revealed that this predictive model for OS was accurate and reliable in stratifying osteosarcoma patients, which was further validated by analyzing the data from GEO datasets (GSE16091 and GSE39058). All these results suggested that this model is clinically useful. Ultimately, an OS prediction nomogram that could help us to predict survival in patients more accurately was constructed.

According to some previously published studies, ferroptosis and FRGs are the crucial regulators of tumor immunity [27]. Thus, the effects of FRG-based risk score on tumor immunity were investigated. It was demonstrated by ESTIMATE that in comparison with the low-risk group, the high-risk group had significantly lower stromal and immune scores, indicating that the high-risk group had remarkably suppressed immune responses. Additionally, it was revealed that compared with the high-risk group, the low-risk group had significantly greater infiltration of CD8+ T cells. Apart from their direct tumor cell-killing activity, CD8+ T cells could also induce ferroptosis within tumor cells [28, 29], which might explain why the prognosis in the low-risk group was significantly better than that in the high-risk group. Compared to the high-risk group, the low-risk group exhibited increased infiltration of M1 and M2 and decreased infiltration of M0 macrophages. We inferred that in comparison with the high-risk group, the low-risk group had a significantly higher proportion of M2 macrophage infiltration that was caused by a larger proportion of M0 cells polarized into M2 cells. It was also demonstrated that almost all the genes encoding immune checkpoint molecules were up-regulated in the low-risk group in comparison with the high-risk group. These immune checkpoint molecules are mainly distributed in activated T cells and antigen-presenting cells. Results of this study demonstrated that macrophages were the main antigen-presenting cells and CD8+ T cells were the chief activated T cells in osteosarcoma. Therefore, it was understandable that the elevated expression of immune checkpoint molecules in the low-risk group was the result of increased infiltration of M2 cells and CD8+ T cells in osteosarcoma.

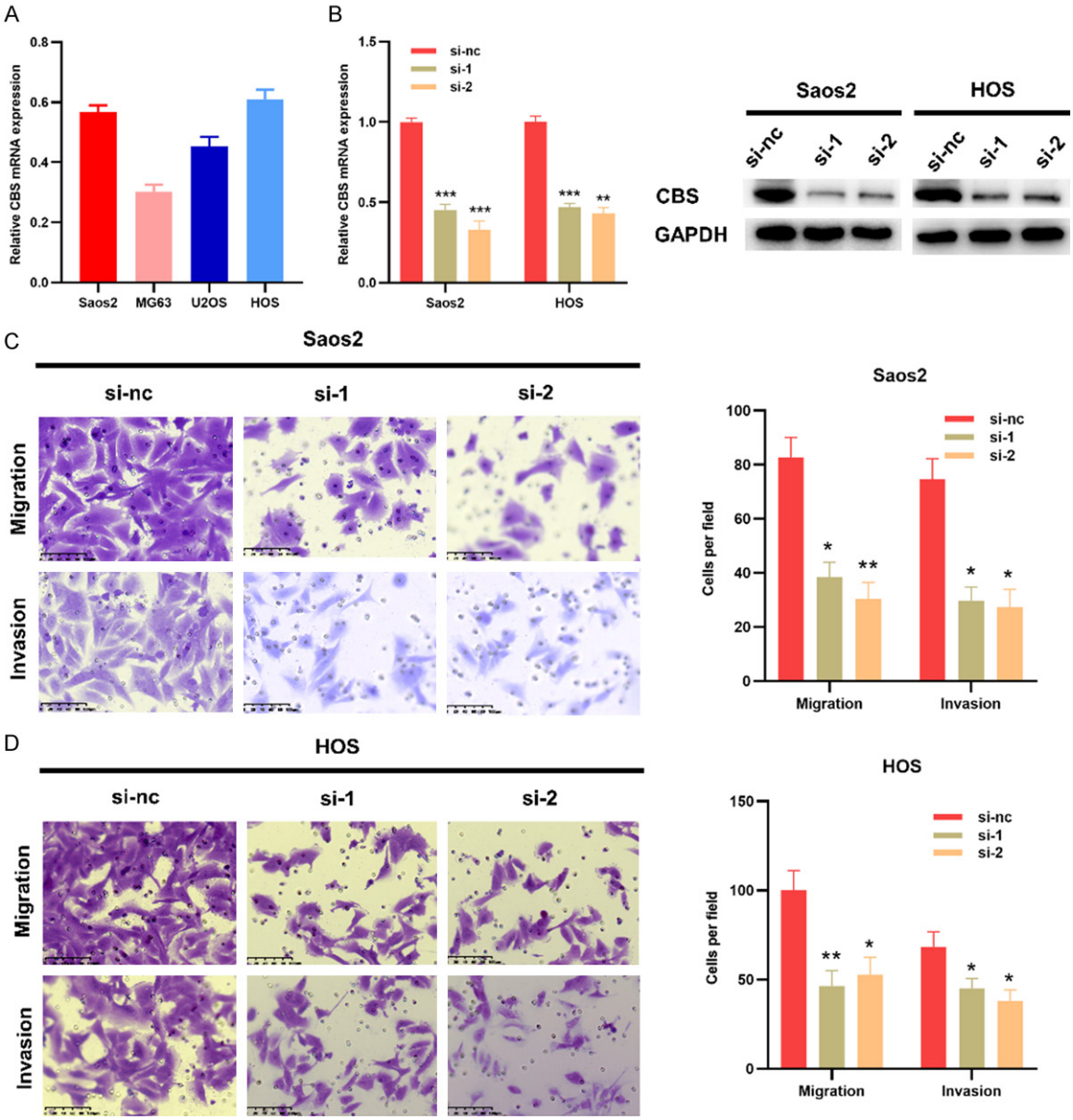

Figure 7. Downregulation of cystathionine β-synthase (*CBS*) weakened the migration and invasion capability of osteosarcoma cells. A. *CBS* mRNA expression level in osteosarcoma cells. B. *CBS* knockdown in Saos2 and HOS cells was confirmed using RT-PCR and western blotting analyses. C, D. Migration and invasion capability of Saos2 and HOS cells was significantly weakened by downregulation of *CBS* expression (*P<0.05, **P<0.01).

Considering all the aforementioned results of this study, we conclude that the interactions between ferroptosis and immune responses are vital in promoting development and progression of osteosarcoma.

Subsequently, potential functions and the likely related mechanisms of FRGs in osteosarcoma were investigated. It was revealed through GSVA that significant differences between risk groups mainly lied in antigen processing and presentation, primary immunodeficiency, NK cell-mediated cytotoxicity, lysosomes, and B cell receptor signaling pathway. By constructing a PPI network, we identified hub genes that included *TP53*, *HMOX1*, *SLC7A11*, *HRAS*, *VEGFA*, and *TXNRD1*, all of which had been reported to play crucial roles in osteosarcoma [30-33]. Additionally, *G6PD* was also indispensable for the growth of osteosarcoma cells [34].

Unlike the clear roles of these molecules in osteosarcoma, roles played by CBS in osteosarcoma remain unclear. According to a recent study, CBS expression leads to the metastasis of osteosarcoma cells to the lung [35]. By performing *in vitro* experiments, we demonstrated that the invasion and migration capabilities of osteosarcoma cells were significantly inhibited after CBS was knocked down. Thus, CBS plays important roles in osteosarcoma progression, and it has the potential of serving as a prognostic biomarker for this cancer. Nevertheless, further studies are still warranted to facilitate in-depth understanding the underlying mechanisms related to FRGs.

In conclusion, a comprehensive study investigating the prognostic significance of potential functions of differentially expressed FRGs in osteosarcoma was accomplished. A model based on four FRGs that could reliably predict outcomes in patients with osteosarcoma was established and validated. Additionally, it was also revealed that the interactions between ferroptosis and immune responses played vital roles in progression of osteosarcoma and these interactions could be potential targets for developing novel therapeutic strategies and improving prognoses in patients with osteosarcoma.

Acknowledgements

We appreciate the opening of the TCGA, GEO, and TARGET databases to researchers.

Disclosure of conflict of interest

None.

Address correspondence to: Jie Yao and Huimin Zhu, Minimally Invasive Spinal Surgery Center, Luoyang Orthopedic-Traumatological Hospital of Henan Province (Henan Provincial Orthopedic Hospital), Zhengzhou 450016, China. E-mail: yaojie110120@163.com (JY); wjzhuhm@126.com (HMZ)

References

[1] Harrison DJ, Geller DS, Gill JD, Lewis VO and Gorlick R. Current and future therapeutic approaches for osteosarcoma. Expert Rev Anticancer Ther 2018; 18: 39-50.

[2] Kumar R, Kumar M, Malhotra K and Patel S. Primary osteosarcoma in the elderly revisited: current concepts in diagnosis and treatment. Curr Oncol Rep 2018; 20: 13.

[3] Huang X, Zhao J, Bai J, Shen H, Zhang B, Deng L, Sun C, Liu Y, Zhang J and Zheng J. Risk and clinicopathological features of osteosarcoma metastasis to the lung: a population-based study. J Bone Oncol 2019; 16: 100230.

[4] Kager L, Tamamyan G and Bielack S. Novel insights and therapeutic interventions for pediatric osteosarcoma. Future Oncol 2017; 13: 357-368.

[5] Stockwell BR, Friedmann Angeli JP, Bayir H, Bush AI, Conrad M, Dixon SJ, Fulda S, Gascón S, Hatzios SK, Kagan VE, Noel K, Jiang X, Linkermann A, Murphy ME, Overholtzer M, Oyagi A, Pagnussat GC, Park J, Ran Q, Rosenfeld CS, Salnikow K, Tang D, Torti FM, Torti SV, Toyokuni S, Woerpel KA and Zhang DD. Ferroptosis: a regulated cell death nexus linking metabolism, redox biology, and disease. Cell 2017; 171: 273-285.

[6] Liang C, Zhang X, Yang M and Dong X. Recent progress in ferroptosis inducers for cancer therapy. Adv Mater 2019; 31: e1904197.

[7] Hassannia B, Vandenabeele P and Vanden Berghe T. Targeting ferroptosis to iron out cancer. Cancer Cell 2019; 35: 830-849.

[8] Yu H, Guo P, Xie X, Wang Y and Chen G. Ferroptosis, a new form of cell death, and its relationships with tumourous diseases. J Cell Mol Med 2017; 21: 648-657.

[9] Jiang L, Kon N, Li T, Wang SJ, Su T, Hibshoosh H, Baer R and Gu W. Ferroptosis as a p53-mediated activity during tumour suppression. Nature 2015; 520: 57-62.

[10] Sun X, Ou Z, Chen R, Niu X, Chen D, Kang R and Tang D. Activation of the p62-Keap1-NRF2 pathway protects against ferroptosis in hepatocellular carcinoma cells. Hepatology 2016; 63: 173-184.

[11] Zhu S, Zhang Q, Sun X, Zeh HJ 3rd, Lotze MT, Kang R and Tang D. HSPA5 regulates ferroptotic cell death in cancer cells. Cancer Res 2017; 77: 2064-2077.

[12] Sun X, Ou Z, Xie M, Kang R, Fan Y, Niu X, Wang H, Cao L and Tang D. HSPB1 as a novel regulator of ferroptotic cancer cell death. Oncogene 2015; 34: 5617-5625.

[13] Liang M, Chen M, Zhong Y, Singh S and Singh S. Construction of a prognostic model in lung adenocarcinoma based on ferroptosis-related genes. Front Genet 2021; 12: 739520.

[14] Xu Z, Xie Y, Mao Y, Huang J, Mei X, Song J, Sun Y, Yao Z and Shi W. Ferroptosis-related gene signature predicts the prognosis of skin cutaneous melanoma and response to immunotherapy. Front Genet 2021; 12: 758981.

[15] Li XX, Xiong L, Wen Y and Zhang ZJ. Comprehensive analysis of the tumor microenviron-

ment and ferroptosis-related genes predict prognosis with ovarian cancer. Front Genet 2021; 12: 774400.
[16] Zhao J, Liu Z, Zheng X, Gao H and Li L. Prognostic model and nomogram construction based on a novel ferroptosis-related gene signature in lower-grade glioma. Front Genet 2021; 12: 753680.
[17] Paoloni M, Davis S, Lana S, Withrow S, Sangiorgi L, Picci P, Hewitt S, Triche T, Meltzer P and Khanna C. Canine tumor cross-species genomics uncovers targets linked to osteosarcoma progression. BMC Genomics 2009; 10: 625.
[18] Ritchie ME, Phipson B, Wu D, Hu Y, Law CW, Shi W and Smyth GK. Limma powers differential expression analyses for RNA-sequencing and microarray studies. Nucleic Acids Res 2015; 43: e47.
[19] Maag JLV. gganatogram: an R package for modular visualisation of anatograms and tissues based on ggplot2. F1000Res 2018; 7: 1576.
[20] Galili T, O'Callaghan A, Sidi J and Sievert C. heatmaply: an R package for creating interactive cluster heatmaps for online publishing. Bioinformatics 2018; 34: 1600-1602.
[21] Kelly AD, Haibe-Kains B, Janeway KA, Hill KE, Howe E, Goldsmith J, Kurek K, Perez-Atayde AR, Francoeur N, Fan JB, April C, Schneider H, Gebhardt MC, Culhane A, Quackenbush J and Spentzos D. MicroRNA paraffin-based studies in osteosarcoma reveal reproducible independent prognostic profiles at 14q32. Genome Med 2013; 5: 2.
[22] Newman AM, Liu CL, Green MR, Gentles AJ, Feng W, Xu Y, Hoang CD, Diehn M and Alizadeh AA. Robust enumeration of cell subsets from tissue expression profiles. Nat Methods 2015; 12: 453-457.
[23] Yu G, Wang LG, Han Y and He QY. clusterProfiler: an R package for comparing biological themes among gene clusters. Omics 2012; 16: 284-287.
[24] Hänzelmann S, Castelo R and Guinney J. GSVA: gene set variation analysis for microarray and RNA-seq data. BMC Bioinformatics 2013; 14: 7.
[25] Li J, Su L, Xiao X, Wu F, Du G, Guo X, Kong F, Yao J and Zhu H. Development and validation of novel prognostic models for immune-related genes in osteosarcoma. Front Mol Biosci 2022; 9: 828886.
[26] Xie Y, Hou W, Song X, Yu Y, Huang J, Sun X, Kang R and Tang D. Ferroptosis: process and function. Cell Death Differ 2016; 23: 369-379.
[27] Tang R, Xu J, Zhang B, Liu J, Liang C, Hua J, Meng Q, Yu X and Shi S. Ferroptosis, necroptosis, and pyroptosis in anticancer immunity. J Hematol Oncol 2020; 13: 110.
[28] Wang W, Green M, Choi JE, Gijón M, Kennedy PD, Johnson JK, Liao P, Lang X, Kryczek I, Sell A, Xia H, Zhou J, Li G, Li J, Li W, Wei S, Vatan L, Zhang H, Szeliga W, Gu W, Liu R, Lawrence TS, Lamb C, Tanno Y, Cieslik M, Stone E, Georgiou G, Chan TA, Chinnaiyan A and Zou W. CD8(+) T cells regulate tumour ferroptosis during cancer immunotherapy. Nature 2019; 569: 270-274.
[29] Lang X, Green MD, Wang W, Yu J, Choi JE, Jiang L, Liao P, Zhou J, Zhang Q, Dow A, Saripalli AL, Kryczek I, Wei S, Szeliga W, Vatan L, Stone EM, Georgiou G, Cieslik M, Wahl DR, Morgan MA, Chinnaiyan AM, Lawrence TS and Zou W. Radiotherapy and immunotherapy promote tumoral lipid oxidation and ferroptosis via synergistic repression of SLC7A11. Cancer Discov 2019; 9: 1673-1685.
[30] Zhu H, Klement JD, Lu C, Redd PS, Yang D, Smith AD, Poschel DB, Zou J, Liu D, Wang PG, Ostrov D, Coant N, Hannun YA, Colby AH, Grinstaff MW and Liu K. Asah2 represses the p53-Hmox1 Axis to protect myeloid-derived suppressor cells from ferroptosis. J Immunol 2021; 206: 1395-1404.
[31] Park HR, Jung WW, Bertoni F, Bacchini P, Park JH, Kim YW and Park YK. Molecular analysis of p53, MDM2 and H-ras genes in low-grade central osteosarcoma. Pathol Res Pract 2004; 200: 439-445.
[32] Luo Y, Gao X, Zou L, Lei M, Feng J and Hu Z. Bavachin induces ferroptosis through the STAT3/P53/SLC7A11 axis in osteosarcoma cells. Oxid Med Cell Longev 2021; 2021: 1783485.
[33] Huang S, Zhu X, Ke Y, Xiao D, Liang C, Chen J and Chang Y. LncRNA FTX inhibition restrains osteosarcoma proliferation and migration via modulating miR-320a/TXNRD1. Cancer Biol Ther 2020; 21: 379-387.
[34] Wang X, Chen K and Zhao Z. LncRNA OR3A4 Regulated the growth of osteosarcoma cells by modulating the miR-1207-5p/G6PD signaling. Onco Targets Ther 2020; 13: 3117-3128.
[35] Gong L, Sun X, Zhang M, Du J, Ding Y and Jin H. The expression of hydrogen sulfide-producing enzymes in primary and lung metastatic osteosarcoma. Histol Histopathol 2022; 18438.

Table S2. The sequences of primer and siRNA oligonucleotides

CBS	F	5'-GGCCAAGTGTGAGTTCTTCAA-3'
	R	5'-GGCTCGATAATCGTGTCCCC-3'
GAPDH	F	5'-ACAACTTTGGTATCGTGGAAG-3'
	R	5'-GCCATCACGCCACAGTTTC-3'
si-1		5'-GGAAGAAGUUCGGCCUGAATT-3'
si-2		5'-CCAUUGACUUGCUGAACUUTT-3'

Table S3. Differentially expressed ferroptosis-related gene

Gene	logFC	AveExpr	t	*P*.Value	B
SAT1	3.589841	9.230784	14.22946	5.78E-11	15.44455
NQO1	-2.78865	7.012353	-10.8712	3.85E-09	11.28123
AHCY	-2.02833	8.532941	-9.20331	4.55E-08	8.792027
ENPP2	5.208452	9.062647	8.974364	6.55E-08	8.424519
SUV39H1	-1.60952	7.631176	-8.79489	8.74E-08	8.131778
SLC7A11	-1.82524	5.203529	-8.3523	1.81E-07	7.392106
BRD7	-1.42905	7.456471	-8.00444	3.27E-07	6.792577
NF2	-1.47915	5.216639	-7.68698	5.69E-07	6.231198
HRAS	-2.20786	7.501765	-7.58305	6.84E-07	6.044411
ZFP36	1.428333	8.042941	7.511918	7.77E-07	5.915723
SLC7A5	-2.19429	8.522941	-7.28063	1.18E-06	5.492469
AURKA	-1.51786	7.1	-6.83269	2.69E-06	4.651724
TFAM	-1.56587	6.148235	-6.63381	3.93E-06	4.26958
TXNRD1	-1.52524	9.210588	-6.43923	5.70E-06	3.890495
CS	-1.11762	9.522941	-5.85695	1.80E-05	2.726183
TMBIM4	1.027619	7.942941	5.679109	2.57E-05	2.362058
CAV1	-2.07357	8.492353	-5.61781	2.91E-05	2.235672
CISD1	-1.7119	7.403529	-5.54242	3.40E-05	2.079637
P4HB	1.260357	11.03294	5.503797	3.68E-05	1.999457
TXNIP	2.523333	9.118039	5.434603	4.24E-05	1.855388
TSC22D3	1.63881	7.737941	5.313768	5.45E-05	1.602559
FH	-1.22714	7.459412	-5.29704	5.64E-05	1.567445
SLC1A5	-1.00976	7.651765	-5.23603	6.40E-05	1.439104
CEBPG	-2.05952	6.300588	-4.97479	0.000111	0.88556
WIPI1	1.913095	7.698824	4.838936	0.000148	0.595386
G6PD	-1.9681	7.005882	-4.49803	0.000307	-0.13836
CDKN2A	1.818889	6.81902	4.417111	0.000365	-0.31344
AGPS	-1.75524	6.661176	-4.17144	0.000622	-0.84618
MMP13	4.010476	8.739412	4.074713	0.000768	-1.05617
VEGFA	1.839048	8.293676	3.871691	0.001196	-1.49665
TP53	-1.42024	5.427059	-3.80248	0.001392	-1.64656
GOT1	-1.24786	7.642353	-3.71574	0.001682	-1.83413
PSAT1	-2.0831	7.981176	-3.69855	0.001747	-1.87125
CBS	-1.79786	6.659412	-3.67181	0.001852	-1.92896
DDIT4	2.171667	8.811765	3.64257	0.001974	-1.99202
FXN	-1.05238	6.62	-3.55945	0.002367	-2.17091
DLD	-1.08333	8.741176	-3.4132	0.003256	-2.48411
GSK3B	-1.12	7.577647	-3.31209	0.004057	-2.69924
CDCA3	-1.08	6.780588	-3.30327	0.004135	-2.71795

CYBB	1.262619	5.806471	3.221716	0.004935	-2.89034
CD44	-1.14479	7.391397	-3.18821	0.005307	-2.96088
CTSB	1.284107	9.7325	3.140018	0.005889	-3.06199
LAMP2	1.060238	7.996471	3.088359	0.006582	-3.16993
YWHAE	-1.26607	8.117353	-3.03797	0.007336	-3.27472
MTDH	1.127381	9.095098	2.992869	0.008081	-3.36808
SCP2	1.117381	8.623529	2.962658	0.00862	-3.43037
PEX2	1.008571	8.300588	2.663553	0.016231	-4.03499
RRM2	-1.12583	9.436176	-2.54696	0.020681	-4.26368
SLC38A1	-1.40024	7.233529	-2.33505	0.031866	-4.66703
HMOX1	1.119048	7.958235	2.179032	0.043472	-4.95237